Laser plasma spectroscopy of Al-Cu-Fe quasicrystal and alloy

M. Satta[1,2], X Zeng[3], X. Mao[3], S. S. Mao[3], R. E. Russo[3], A. Giardini[1], and A. Mele[1,*]

[1] *Dipartimento di Chimica, Universita' di Roma "La Sapienza", P.le A. Moro 5, 00185, Roma, Italy*

[2] *Istituto Metodologie Inorganiche e Plasmi - CNR, via Loja, Tito Scalo, PZ 85050, Italy*

[3] *Lawrence Berkeley National Laboratory, MS 70-108B, Berkeley, CA 94720, USA*

September 25, 2002

Abstract

Electron number density and temperature were determined from laser induced plasma produced by irradiating Al-Cu-Fe targets of a quasicrystal and of an alloy of similar composition. The Al(I) atomic emission spectra of the two systems were measured as a function of distance from the target and of the time delay after laser irradiation. Differences of plasma characteristics were observed for laser ablation of quasicrystal and alloy targets, and the results were interpreted on the basis of different plasma formation mechanism for the two systems.

INDEX HEADING: Laser ablation, quasicrystal, plasma spectroscopy.

* corresponding author, *aldo.mele@uniroma1.it*

1. Introduction

Pulsed laser irradiation of metal targets typically produces a luminous plasma above the solid surface during the removal of material[1, 2]. The strong coupling between laser photons and the surface of target material yields plasma emission spectra which consist of neutral and ionic lines together with a continuum background, reflecting the elemental composition of the target material. Plasma formation depends on laser characteristics such as intensity, wavelength, pulse duration, as well as background pressure[3].

Many aspects of laser ablation processes are not well defined, especially the correlation between the plasma characteristics and the target components. Electronic number density and temperature of the laser induced plasma are of great interest for understanding the interaction of a laser beam with a solid target, and for the application of laser ablation sampling for qualitative and quantitative analysis of multi-component materials. Plasma characteristics can provide an insight for optimization of the process of laser ablation for specific purposes. One powerful technique of determining electron number densities and temperatures in a laser plasma comes from spectroscopic measurements of the Stark broadening. Spectral line widths result from the interaction between a radiator and its surrounding particles, which is related to the rate of effective collisions, a dominant mechanism for line broadening. In addition to broadening, there is also a shift (usually toward increasing wavelength) of spectral line center away from the position as the electron density N_e approaches zero[4].

In this work laser induced plasmas, at atmospheric pressure, from an Al-Cu-Fe quasicrystal (QC) and an alloy of similar composition are examined by measuring plasma emission spectra and calculating electron number densities and temperatures. The idea is that structural differences of the two systems may play a role on the mechanism of laser ablation and on the characteristics of the

laser produced plasma. The QC and the alloy have virtually the same composition, but their elements are bound together in a different fashion[5].

2. Experiments

2.1 Instrumentation

A diagram of the experimental system[6] is shown in fig. 1. The laser source is a quadrupled Nd:YAG laser (Coherent, Infinity) operating at 266 nm with 3 ns pulse duration. A 90/10% beam splitter was used to observe the laser pulse temporal shape using a fast UV photodiode coupled to a 1.5 GHz oscilloscope (LeCory-9632). The laser pulse energy was measured using a pyroelectric detector and a joulemeter after passing through a 50/50% beam splitter. A group of mirrors was used to direct the laser beam perpendicularly onto the target surface. After focusing with a plano-convex quartz lens (f = 20 cm), ~ 50 μm spot diameter could be achieved. The irradiance was in the range of 6 to 60 GW/cm^2. All data represent single laser pulse ablation on a clean sample surface. The sample was mounted on an *xyz* micrometer translation stage so that the sampling location could be changed after each laser pulse.

For spectroscopic observation, a bi-convex quartz lens (f = 15 cm) was used to image the laser induced plasma onto the entrance slit of a Czerny-Turner spectrometer with focal length 270 mm (Spex Industries Model 270M). The spectra were detected by an intensified charge-coupled device (ICCD) system which consists of a thermoelectrically cooled CCD (EG&G/Princeton Applied Research, Model OMA VISION) with 512 pixels and a microchannel plate (MCP) as image intensifier. The combination of spectrometer with this detection system provided a spectral window of ~ 13 nm and resolution of typically 0.125 nm, when the entrance slit width of 20 μm and grating of 1800 grooves per mm were used. The dark current background of the CCD detector was subtracted from the measured spectroscopic data for each measurement. Gating the ICCD and

changing the delay time enables the spectra to be temporally resolved. The gate width and time delay were controlled by the OMA SPEC 4000 software (EG&G/Princeton Applied Research), and synchronously triggered from the Q-switched signal produced by the Nd:YAG laser. A photo diode and a digitizing oscilloscope were used to measure the accurate time delay. The gate width was set at 30 ns, and the delay time could vary from 10 ns to 1500 ns.

The Induced Coupled Plasma-Mass Spectrometry (ICP-MS) detection of the aluminum yield was performed by irradiating the targets by single laser pulse and the signal intensity data acquired in the time resolved mode at different power densities [5].

The Al-Cu-Fe multi-component samples used in this study were a quasicrystal $Al_{65}Cu_{23}Fe_{12}$ and a metallic alloy $Al_{70}Cu_{20}Fe_{10}$, both with nearly the same metal components but different structural features[5]. The targets were polished and cleaned with methanol before ablation. Distance and time dependent emission spectra[6] were obtained by observing plasma emission at different locations with respect to unablated sample surface, after laser irradiation of the sample at different time delays.

3. Results and Discussion

3.1 Theory and spectra characteristics

The atomic and ionic densities present in the plasma produced by laser ablation follow a fast dynamics in time and space domains. This rapid plasma transformation is reflected in the emission-line changes as a function of time and distance. In regions near the target surface and at short time delays, the emission spectrum is a continuum, reflecting the microscopic mechanism of recombination of electron with ions (free-bound) and scattering of electrons with atoms and ions (free-free). After this first transient period and at intermediate regions in space away from the target

surface, a spectrum characterized by distinct emission-lines can be observed, which comes from radiative decay of excited species. This domain is defined by a cooling and expansion of the plasma associated with a decrease of electron, atom and ion densities.

In this paper the electron densities of laser plasmas have been determined from Stark-broadening of the emission lines of the spectra. Doppler, Van der Waals and natural broadening are mechanisms of negligible importance in the emission line shift and increase in its Full Width Half Maximum (FWHM)[6]. The emission lines originated from the excited atomic or ionic levels are broadened and perturbed by the plasma electrons. Stark broadening of well isolated lines provides a useful method for estimating the electron density in the plasma. In this case the half-widths $\Delta\lambda_{1/2}$ (nm) of the emission lines depend on the electron density N_e (cm^{-3}) via the electron impact approximation after being corrected for the quasi-static ion broadening,

$$\Delta\lambda_{1/2} = \frac{2WN_e}{10^{16}} + \frac{3.5AWN_e^{5/4}}{10^{20}}\left(1 - \frac{0.75}{\sqrt[3]{N_D}}\right) \quad (1)$$

where W (nm) is the electron impact width parameter and A the ion-broadening parameter (both weakly dependent on temperature). N_D is the number of particles estimated to be in the Debye sphere,

$$N_D = 1.72 \times 10^9 \sqrt{\frac{T^3}{N_e}} \quad (2)$$

where N_e is in cm^{-3} and T in eV.

The broadening of the emission line is associated with a line shift $\Delta\lambda_{shift}$, which for atomic emission is given by,

$$\Delta\lambda_{shift} = D(\frac{N_e}{10^{16}}) \pm 2AW(\frac{N_e}{10})\left(1 - \frac{0.75}{\sqrt[3]{N_D}}\right) \quad (3)$$

where D represents the diffusion coefficients for radiating species.

It has been assumed that $T_e = T_{exc} = T$, with T_e and T_{exc} being the electronic and excitation temperatures respectively. This assumption is valid if the Local Thermal Equilibrium (LTE) hypothesis is considered. Note that the populations follow a Boltzmann distribution depending on T_e instead of T_{exc} even for systems significantly in non-LTE conditions[7]. Obviously in situations far away from the LTE assumption one has to choose emission lines from higher excited levels. Thus if deviation from LTE is not high, only small errors are produced approximating the electron temperature with the excitation temperature.

The LTE condition is satisfied with a lower limit of the electron number density to ensure a high collision rate,

$$N_e \geq 1.4 \times 10^{14} \sqrt{T} \Delta E^3 \quad (4)$$

where ΔE is the energy needed to go from the lower to the upper level. The measured electron number density is higher than this value, which confirms that LTE conditions should prevail.

We applied an iterative procedure to calculate N_e and T by using the inverted equation 1 once with respect to N_e and once to T up to the point of convergence for N_e and T. At each step of the iterative procedure we have accounted for the dependence of W and A from the temperature as

obtained by a quadratic fitting (see tab. I) of the data of reference[8]. At the first step of this procedure, the electron number density is calculated without the contribution of the quasi-static ion broadening (the second term of eq. 1), which is small in our case. At T=8000 and $N_e=5\cdot10^{18}$ its contribution is less then 1%. The eq. 1 thus reduced to:

$$\Delta\lambda_{1/2} = \frac{2WN_e}{10^{16}} \tag{5}$$

This is confirmed by the fact that the broadening parameter $\Delta\lambda_{1/2}$ is not affected from the temperature as can be seen from fig. 2.

The FWHM in different experimental conditions (i.e. at different time-delays and at different distances from the target surface) has been calculated by fitting the experimental emission line with single or double Lorentzian functions,

$$I(\lambda) = I_0 + \frac{2\alpha w}{\pi[4(\lambda-\lambda_c)^2 + w^2]} \tag{6}$$

$$I(\lambda) = I_0 + \frac{2\alpha' w'}{\pi[4(\lambda-\lambda'_c)^2 + w'^2]} + \frac{2\alpha'' w''}{\pi[4(\lambda-\lambda''_c)^2 + w''^2]} \tag{7}$$

where λ_c is the center of the peak, w is FWHM, I_0 is the background level, α the integrated area of emission line, and the $'$ and $''$ suffixes are related to the parameters of the lower and higher energy peaks of Al(I). In the case of the repeated measurements at 95 ns time delay at 40 different distances from the target surface, a statistic has been obtained by calculating the fitting parameters assuming a 10% of errors in the emission intensities measurements.

3.2 Plasma emission and spectra analysis

The Al(I) emission line near 395 nm showing fig. 3 were used for the plasma diagnostics of the Al-Cu-Fe quasicrystal and alloy of approximately of the same composition. The 395 nm lines, superimposed to a continuum, are made of two lines at 394.4 nm and at 396.1 nm arising from 4s ($^2S_{1/2}$) – 3p ($^2P_{1/2}$) and 4s ($^2S_{1/2}$) – 3p ($^2S_{3/2}$) transitions. These lines are completely separated at large distance from the target. The Lorentzian fitting on the 396.1 nm line was used for all calculations. The spectra observed in this region show at a given distance from the target another line at 398 nm which can be attributed to singly ionized A(II). Ion lines have been observed to move faster than neutrals in a laser induced aluminum plasma[9]. The 398 line is present in the spectra at very short distance from the target, and gradually disappears and replaced by emission from exited neutral Al[3,10]. The Stark full width half maximum $\Delta\lambda_{FWHM}$ and the shift $\Delta\lambda_{shift}$ at the 396.1 nm line were deduced by deconvolution of the recorded spectra profile of fig. 3. Other contributions to the spectral line broadening were considered small to be safely neglected. Previous work on the aluminum plasma emission induced by nanosecond and femtosecond have been reported in the literature. These papers investigated time and space resolved laser induced spectroscopy of Al alloy targets[10-12].

We have observed that the plasma emission spectra of the QC and the alloy are composed of, together with Al lines, many Cu and Fe lines. These lines for the last two elements were too many in the ns time delay. The line width was on the order of nm, so we were not able to get any information for Cu and Fe. Al atomic emission has been found to last for several hundreds microseconds. From the curves of fig 4 a,b it can be noted that the Al(I) line emission extends about several millimeters above the target surface. These spectra show the spatial distributions of the plasma emission at 95 ns time delay in air atmosphere. The spectra are similar and in the two systems with a decay time at about a distance d = 5 mm.

The FWHM broadening and the shift of the line center wavelengths were measured on the emission peaks at 396.1 nm. The curves, which were fitted on six repeated experiments have been used for the calculations of the electron number densities as a function of the distance from the target. The trends of the broadening as well of the shift as a function of the distance show both a marked difference between the two systems and it will be discussed in the next paragraph.

3.3 Electron number density, plasma temporal evolution and temperature

The plots of fig. 5 a,b show the electron number density and the temperature as a function of the distance from the target for the QC and the alloy. The values have been obtained from the data of the Stark broadening by using eq. 1. A significant difference between the curves of the alloy and of the QC may be observed. Both systems are characterized by a decrease of N_e and T with distance. The electron number density are larger for the alloy than for the QC. These values are in the range of 10^{18} to 10^{19} cm^{-3} and the temperature around 10^4 K. The Al(I) line is strongly broadened by the Stark effect because of the high electron density of the laser induced plasma which is initially formed at a distance of about 1.4 mm and is extinguished at about 5 mm . The conclusion is that in the same high power density regime 57.2 GW/cm^2, the ejection of electrons as measured by the electron number density, is different for the two systems probably according to their structures.

The temporal evolution of the laser induced plasma has been observed at a power density of 6.37 GW/cm^2 and 0.12GW/cm^2 as shown in the two 3D plots of fig 6 a,b. In these plots, the spectra line broadening, the shift and the continuum emission at six values of the time delay has been evaluated only at the power density of 6.37 GW/cm^2 . The emission spectra at 0.12 GW/cm^2 is very weak and at the limit of detection.

3.4 Mechanism considerations

The electron number density calculated by the plasma characteristics reflects the effects of the coupling between the laser and the solid in the two systems, which in turn depends on the models representing the structures whose feature are extended from the bulk to the surface. Accordingly to their structures we can expect that in the QC the electrons are strongly bound in the valence orbitals, while in the metallic alloy are free to move in the whole structure.

Electron number density and temperature as a function of the time delay after the laser irradiation of the sample are plotted in fig. 7 for the alloy and the QC samples. Individual spectra in fig. 6 show significant changes of their features with time delay. At early stage a continuum represents the emission in the whole wavelength range. At a later stage the emission changes with the formation of the two distinct peaks at 194.4 and 196.1 nm, which extinguish with time delay at about 1000 ns. The electron number density and temperature were calculated from Stark broadening of the 196.1 line as previously reported. It can be seen from fig. 7 that the electron density ranges from 0.83×10^{18} to 6.37×10^{18} cm^3 and the temperature from 4200 up to 8500 K. The time-dependent data for the two systems fit the same curves for the electron number density and for the temperature, indicating that no significant difference exists between the two samples.

The new class of metallic alloys, quasicrystals (QC), was discovered in 1984 by Dan Shechtman[13]. These compounds are described as an aperiodic structure, with a long-range atomic order and electronic quantum states, intermediate between localized and delocalized[14, 15]. The Fermi electrons in a QC are scarce and this leads to a so called pseudo-gap for electron distribution. In this case localized and delocalized modes for the absorbed photon energy can be expected. Metals are represented by the Drude-Fermi model[16, 17], which assumes that the atoms of a metallic element lie

in a given position in the bulk structure where the detached Fermi electrons freely move. Intermetallic alloys, as binary and ternary metallic systems are similarly represented. The electronic quantum states of metals or alloys are thus highly delocalized and described as extended or band-like[17]. This means that there is little opportunity for localization, and the free electron model is no longer valid for this type of material. The electron propagation in the solids in the case of alloy is ballisitic and for the QC non-ballistic[18]. This is in agreement with the electric properties of the QC which show a temperature dependence which is consistent with a crystallographic structure made of clusters of atoms[19].

The laser-target interaction may follow two different routes in the process of plasma formation and laser ablation. This depends on the laser intensity and on the physical properties of the materials such as absorption cross section, electron-lattice strength and thermal conductivity[20]. It can be assumed that in the case of the metallic alloy, the energy of the laser is depositated on delocalized sites and excitation gives rise mainly to electron phonon scattering. In the case of the QC the photon excitation is partly localized, by retaining the absorbed energy at a single site of the chemical bond forming excited vibrational states. This simple view provides an insight of the results of the plasma analysis of the two systems which have been studied in the present work. Let us observe what happens at the two different power density regimes which have been examined. The data show that at 6.0 GW/cm^2 the electron number density and the plasma temperature are approximately the same for the two systems as can be seen in table II. The electron number density and the temperature follow also the same trend with delay time. The target interaction, at the low power density 6.0 GW/cm^2, is not such to make a real distinction between the metallic alloy and the QC. The laser energy deposition process is such to produce the same results.

In the high power density regime of 57.2 GW/cm^2, we found marked changes for the alloy and minor variation for the QC of the electron number density and temperature with respect to the

data at low power density. This trend is likely to be attributed to two distinct mechanisms. In the case of a material such as the alloy, with a weak electron-lattice coupling, the laser-target interaction excites the free electrons of the metallic structures. The electron ejection, measured by electron number density is high as well as the temperature. The case of the QC is different. The electron-lattice coupling strength is high and the effect of the higher power densities on the electron ejection and on the temperature is yet rather moderate. On the other hand, the slight difference in the Al content between the two systems cannot account for such large electron formation from the alloy with respect to the QC. Further the laser ablation yields for the two samples at 60 GW/cm^2 do not show much difference (fig. 8).

4. Conclusion

The detection limits and precision[3,6] and the modeling and the interpretation of the spectroscopy in terms of the characteristics of the plasma are two major concerns of the method of analysis using laser induced plasma spectra. The collisional dynamics within the plasma vapor and the structural properties of the solid are both represented in the plasma spectra. The question is to establish the factors and parameters involved in the analysis of the plasma and their correlation with laser target interaction. A mechanism that could envisage the electron number density, neutral atoms and molecules density and charged particles is actually the final goal of this complex process, which is far from being fully understood. At higher laser energy than that of the vaporization threshold, the laser irradiation produces a luminous vapor plasma light. The species present in the visible plasma are vaporized, excited atoms and singly and multiply charged ions and free electrons. The evolution of the electron number density and the total number of particles removed from the target requires an understanding of the plasma and the target surface components. This is not a

simple task and can be established only with certain approximation, and with careful study of similar material systems like QCs and alloys.

Acknowledgments

This research was supported by the U.S. Department of Energy, Office of Basic Energy Sciences, Chemical Science Division, under contract No. DE-AC03-76SF00098, the Ministero dell'Istruzione, dell'Università e della Ricerca (MIUR) and Consiglio Nazionale delle Ricerche (CNR).

References

(1) J. T. Ready, *Effects of high power laser radiation* (Accademic Press, New York, 1971).

(2) J. Hermann, C. Boulmer-Leforgue and D. Hang, J. Appl. Phys., **83**, 692 (1998).

(3) X. L. Mao, M. A. Shannon, A. J. Fernandez and R. E. Russo, Appl. Spectro., **49**, 1054 (1995).

(4) H. R. Griem, *Plasma Spectroscopy* (McGraw-Hill, New York, 1964).

(5) M. Satta, H. Liu, X. Mao, G. Moretti, R. E. Russo, A. Giardini and A. Mele, Int. J. of Photoenergy, **3**, 123 (2001).

(6) H. C. Liu, X. L. Mao, J. H. Yoo and R. E. Russo, Spectrochim. Acta B , **54**, 1607 (1999).

(7) G. Bastians and R. A. Mangold, Spectrochim. Acta B , **40** 885 (1985).

(8) H. R. Griem, *Spectra line broadening by plasma* (Accademic Press, New York, 1974).

(9) A. Mele, A. Giardini, C. Flamini, A. Latini, S. Orlando and R. Teghil, Proc. Indian Acad. Sci. (Chem. Sci.), **113**, 163 (1998).

(10) B. L. Drogoff, J. Margot, M. Chacker, M. Sabsabi, O. Barthelemy, T. W. Johnston, S. Laville, F. Vidal and Y. van Kaenel, Spectrochim. Acta B **56**, 987 (2001).

(11) M. Sabsabi and P. Cielo, J. Appl. Spectr., **49**, 499 (1995).

(12) C. Colon, G. Haten, E. Verdugo, P. Ruiz and J. Compos, J. Appl. Phys., **73**, 4752 (1993).

(13) D. Schectman, I. Blech, G. Ratios and J. W. Carin, Phys. Rev. Lett., **53**, 1951 (1984).

(14) J. M. Dubois, Physica Scripta, **T79**, 17 (1993).

(15) P. A. Thiel and J. M. Dubois, Nature, **406**, 570 (2000).

(16) N. W. Ashcroft and N. D. Mermin, *Solid State Physics* (CBS Publishing, Philadelphia).

(17) C. Kittel, *Introduction to Solid State Physics* – 7th edition (John Wiley and Sons Inc., New York, 1996).

(18) P. Archamboult, New horizons in quasicrystals, Research and Applications (World Scientific, Singapore, 1996).

(19) E. Rotenberg, W. Theis, K. Horn and P. Gille, Nature, **406** 607 (2000).

(20) C. Flamini, A. Ciccioli, A. Giardini-Guidoni and A. Mele, J. Materials Synthesis and Processing , **9** 143 (2001).

Table I

The parameters used for the plasma temperature and electron number density calculations. Both A and W have been expanded to the second order in temperature T: $a + bT + cT^2$.

	a	b	c
A	0.0435	$-8.12\ 10^{-7}\ K^{-1}$	$1.13\ 10^{-11}\ K^{-2}$
W	$1.15\ 10^{-3}$ nm	$4.23\ 10^{-8}$ nm/K	$-4.97\ 10^{-13}$ nm/K^2

Table II

Comparison of the electron number density and temperature at 6.0 GW/cm^2 and 57.2 GW/cm^2 between the alloy and the QC at a distance d = 0.275 mm and time delay 100 ns.

		6.0 GW/cm^2	57.2 GW/cm^2
N_e (10^{18} cm^{-3})	QC	2.6	4.4
	Alloy	3.0	9.0
T(K)	QC	6300	7500
	Alloy	6600	9500

Figure captions:

FIG. 1 : Schematic system for spectroscopic measurements of laser induced plasmas.

FIG. 2 : 3D plot of the Al(I) line broadening at 395.6 nm as a function of the electron number density and temperature according to eq. 1.

FIG. 3 : Emission spectra of Al(I) of QC and alloy and Lorentzian fitting at a power density 57.2 GW/cm^2 and at a distance from the target of 1 mm and 3 mm at a time delay of 95 ns.

FIG. 4: 3D plots of the emission spectra as a function of the distance from the target and wavelength for the alloy (a) and the QC (b). Time delay 95 ns. power density = 57.2 GW/cm^2 .

FIG. 5: Electron number density, and in the inset the temperature of alloy and QC as a function of target distance at a power density of 57.2 GW/cm^2 at a time delay of 95 ns.

FIG. 6: Temporal evolution of the Al(I) spectra at two different power density at a distance of 2.5mm.

FIG. 7 : Temporal evolution of plasma electron number density and temperature for QC and alloy sample at a power density of 6.0 GW/cm^2 and target distance of 2.5 mm. The errors have been estimated assuming an error of 10% ob the $\Delta\lambda_{1/2}$.

FIG. 8: Aluminum yields (ICP-MS intensity) of laser ablated QC and alloy.

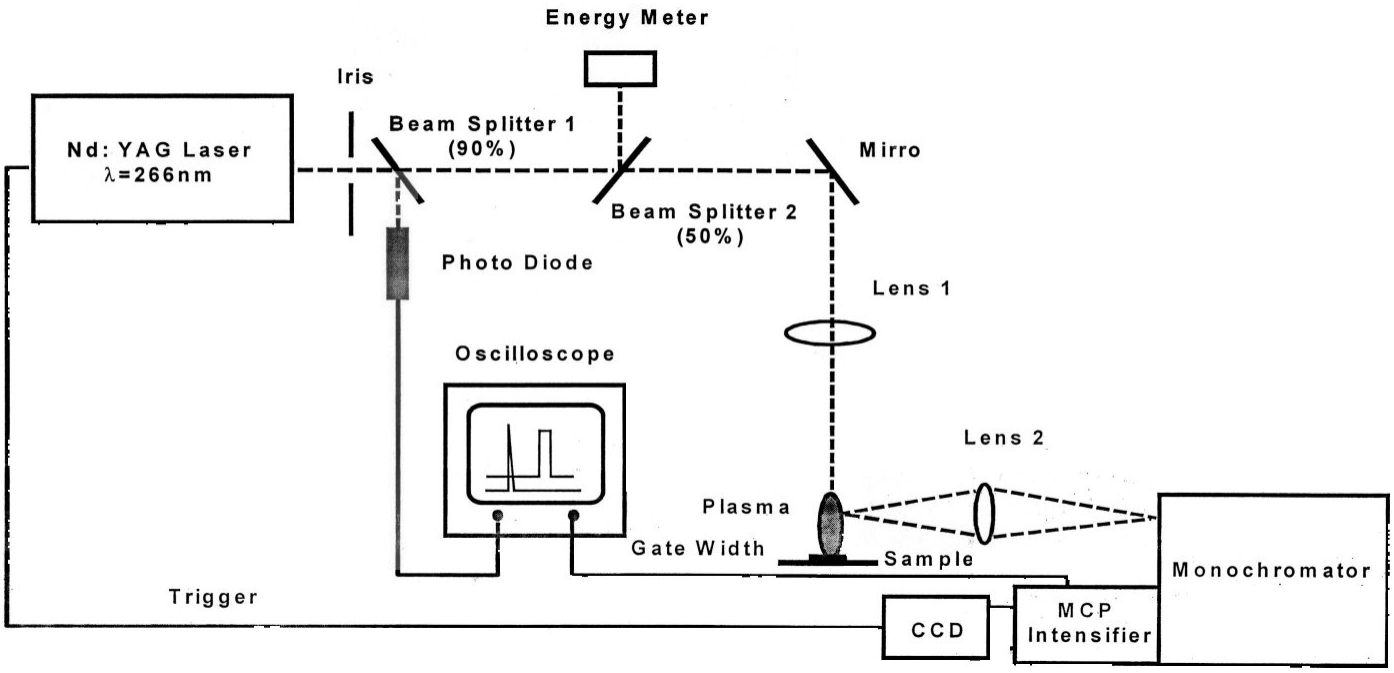
Energy Meter
Iris
Nd: YAG Laser
λ=266nm
Beam Splitter 1
(90%)
Mirro
Beam Splitter 2
(50%)
Photo Diode
Lens 1
Oscilloscope
Lens 2
Plasma
Gate Width
Sample
Monochromator
Trigger
CCD
MCP
Intensifier

Figure 1

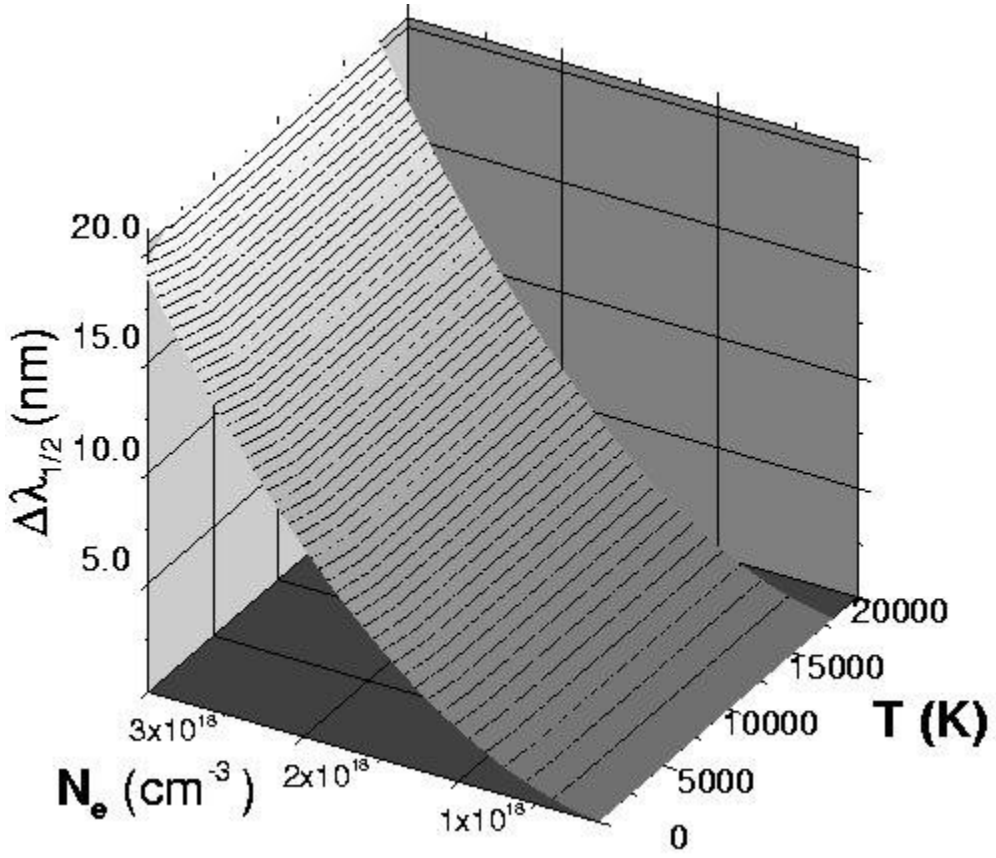
20.0
15.0
10.0
5.0
$\Delta\lambda_{1/2}$ (nm)
3x10^{18}
2x10^{18}
1x10^{18}
N_e (cm^{-3})
20000
15000
10000
5000
0
T (K)

Figure 2

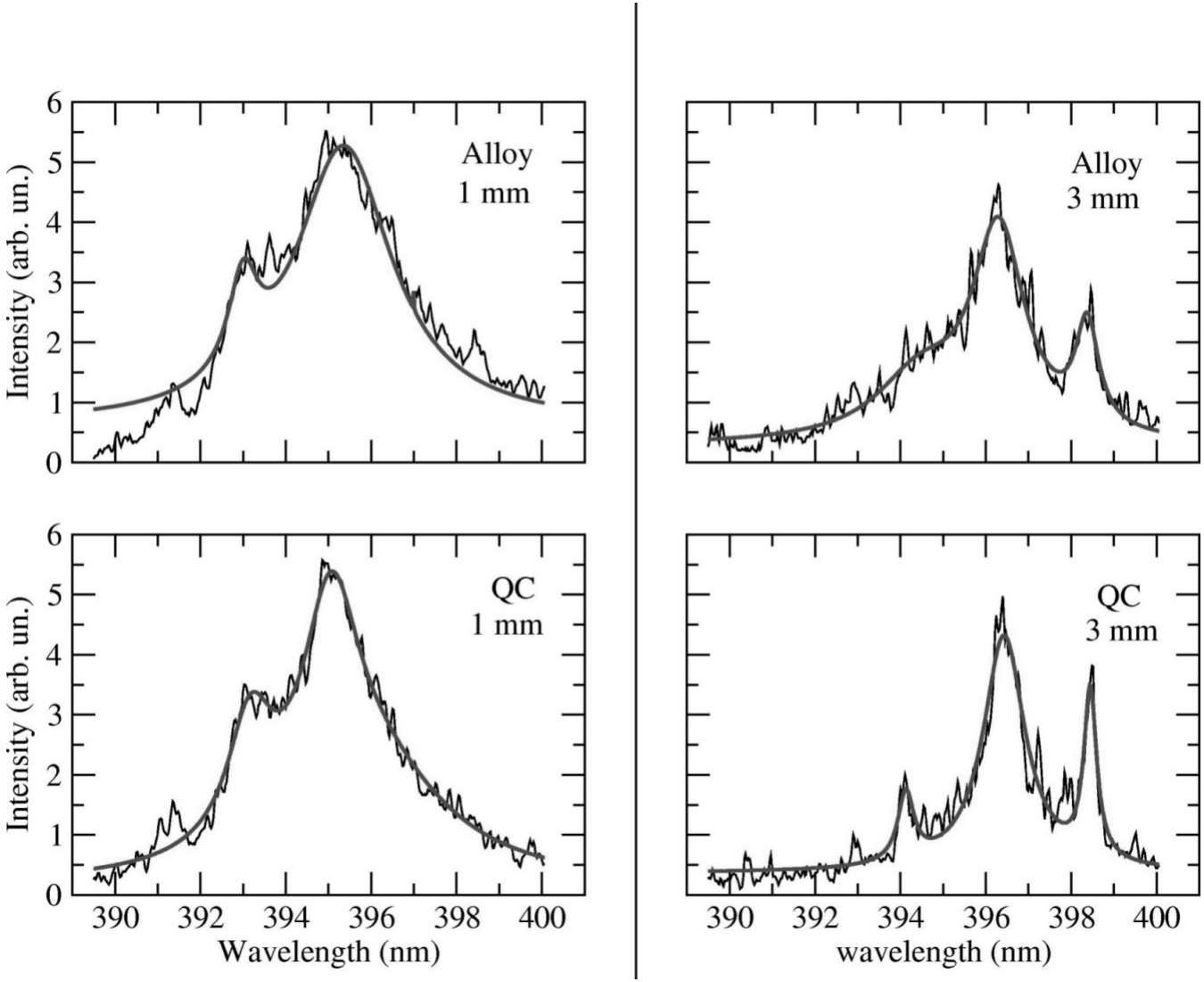
Alloy
1 mm
Alloy
3 mm
QC
1 mm
QC
3 mm
Intensity (arb. un.)
Intensity (arb. un.)
0
1
2
3
4
5
6
390
392
394
396
398
400
Wavelength (nm)
wavelength (nm)

Figure 3

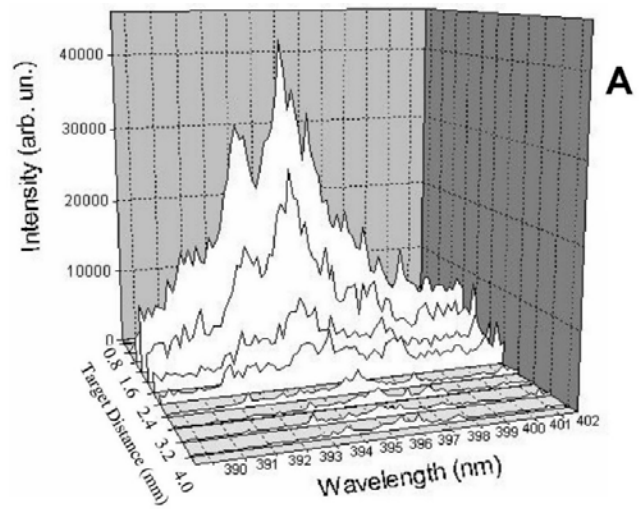
A
Intensity (arb. un.)
40000
30000
20000
10000
0
Target Distance (mm)
0.8
1.6
2.4
3.2
4.0
390 391 392 393 394 395 396 397 398 399 400 401 402
Wavelength (nm)

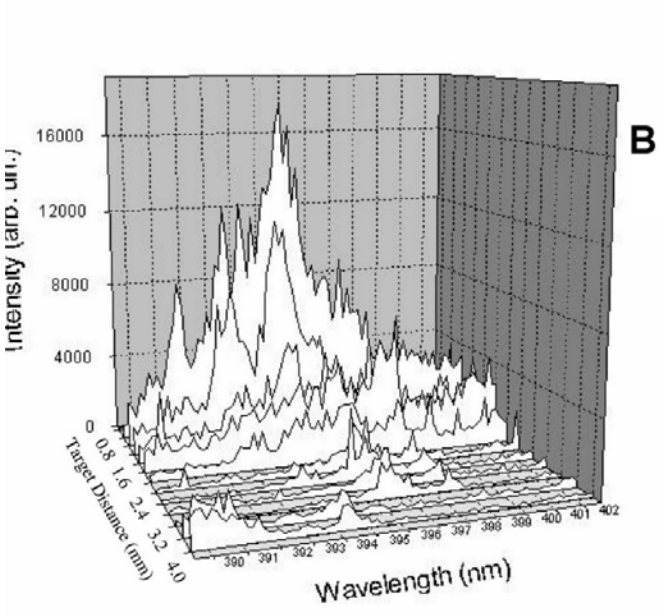
B
16000
12000
8000
4000
0
Target Distance (mm)
0.8
1.6
2.4
3.2
4.0
390 391 392 393 394 395 396 397 398 399 400 401 402
Wavelength (nm)

Figure 4

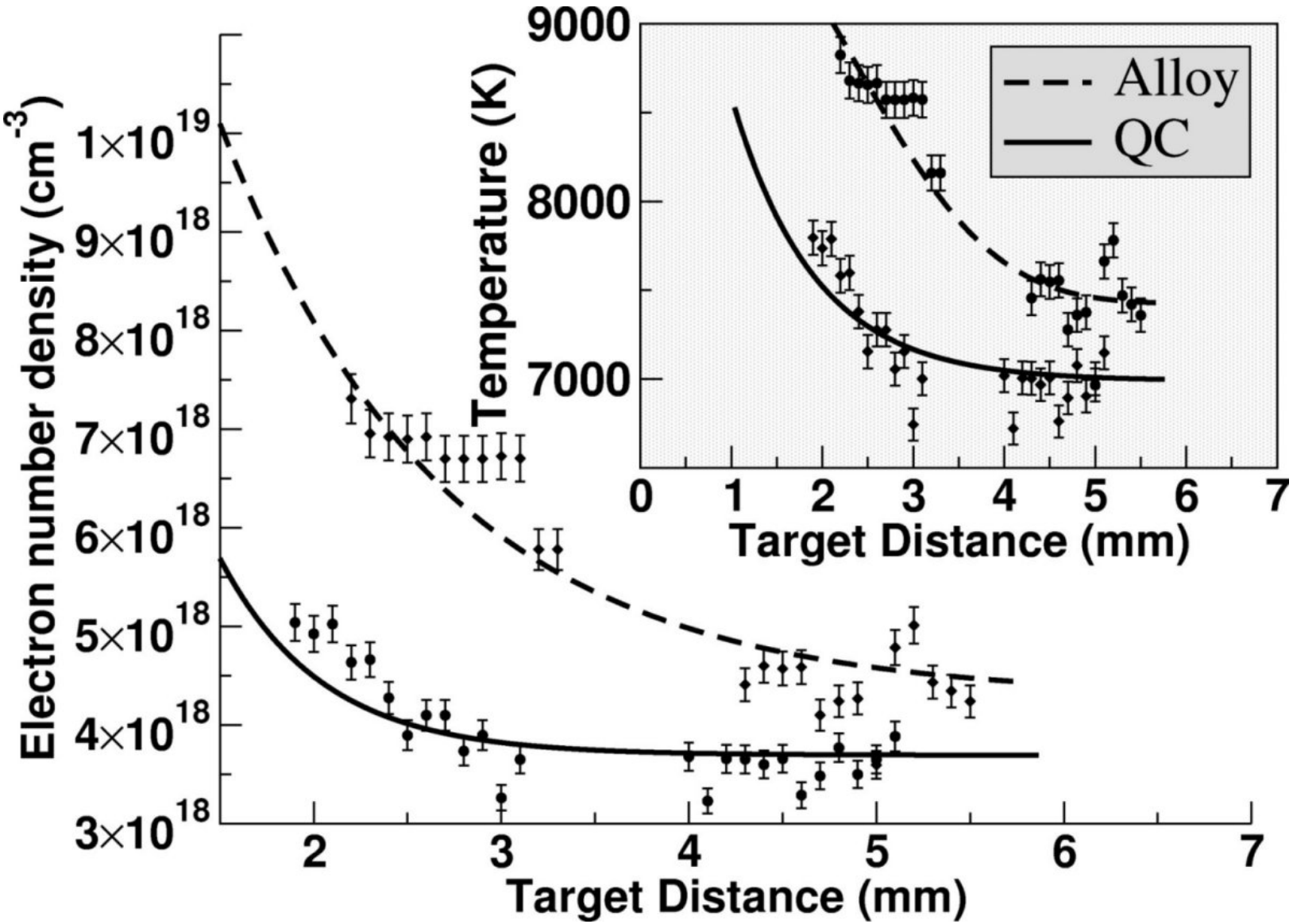
Electron number density (cm^{-3})
1×10^{19}
9×10^{18}
8×10^{18}
7×10^{18}
6×10^{18}
5×10^{18}
4×10^{18}
3×10^{18}
2
3
4
5
6
7
Target Distance (mm)
Temperature (K)
9000
8000
7000
Alloy
QC
0
1
2
3
4
5
6
7
Target Distance (mm)

Figure 5

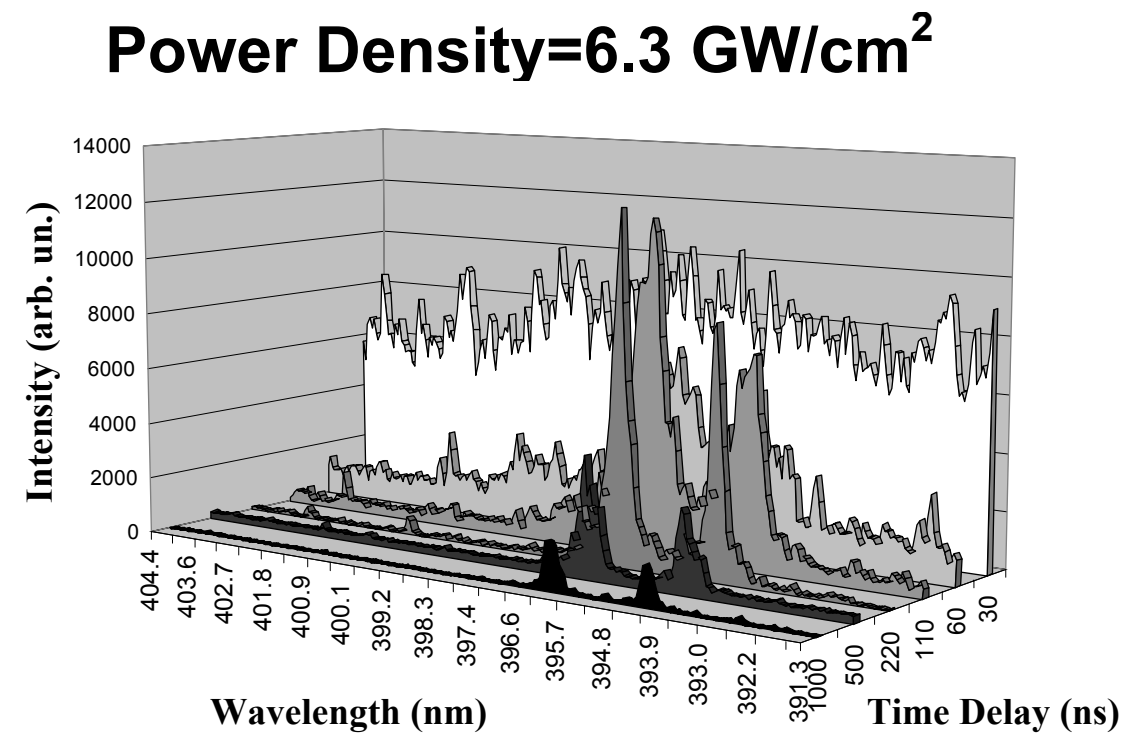
Power Density=6.3 GW/cm2
Intensity (arb. un.)
14000
12000
10000
8000
6000
4000
2000
0
404.4
403.6
402.7
401.8
400.9
400.1
399.2
398.3
397.4
396.6
395.7
394.8
393.9
393.0
392.2
391.3
Wavelength (nm)
1000
500
220
110
60
30
Time Delay (ns)

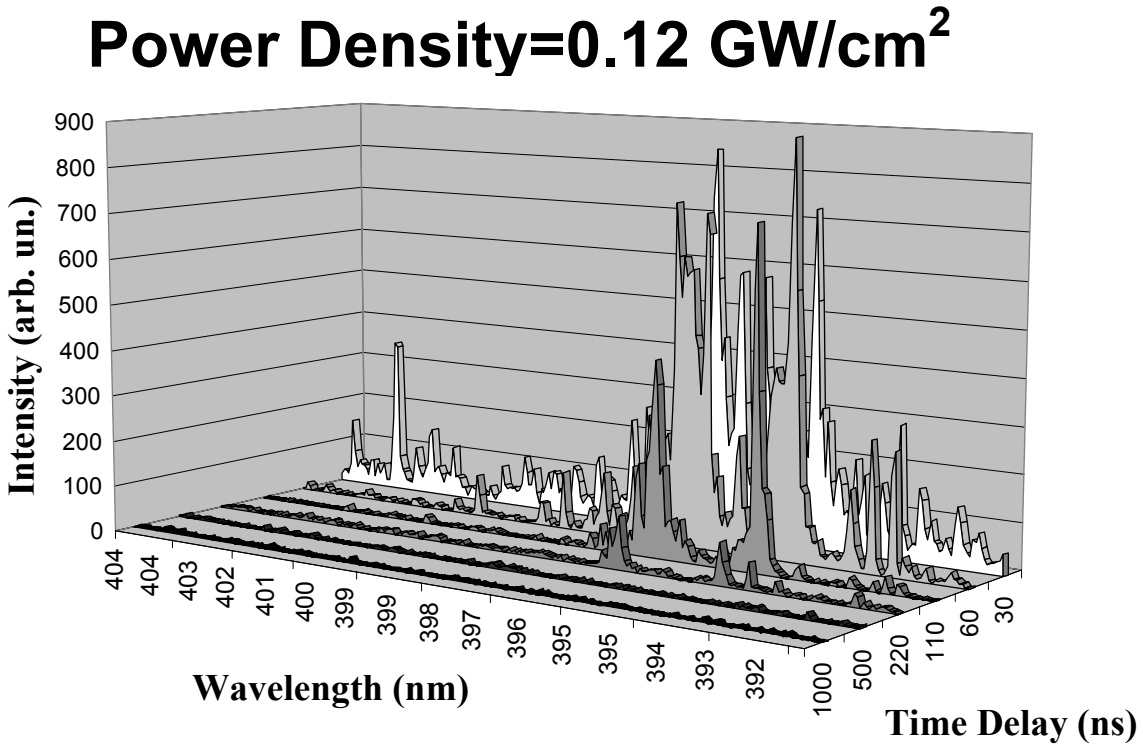
Power Density=0.12 GW/cm2
Intensity (arb. un.)
900
800
700
600
500
400
300
200
100
0
404
404
403
402
401
400
399
399
398
397
396
395
395
394
393
392
Wavelength (nm)
1000
500
220
110
60
30
Time Delay (ns)

Figure 6

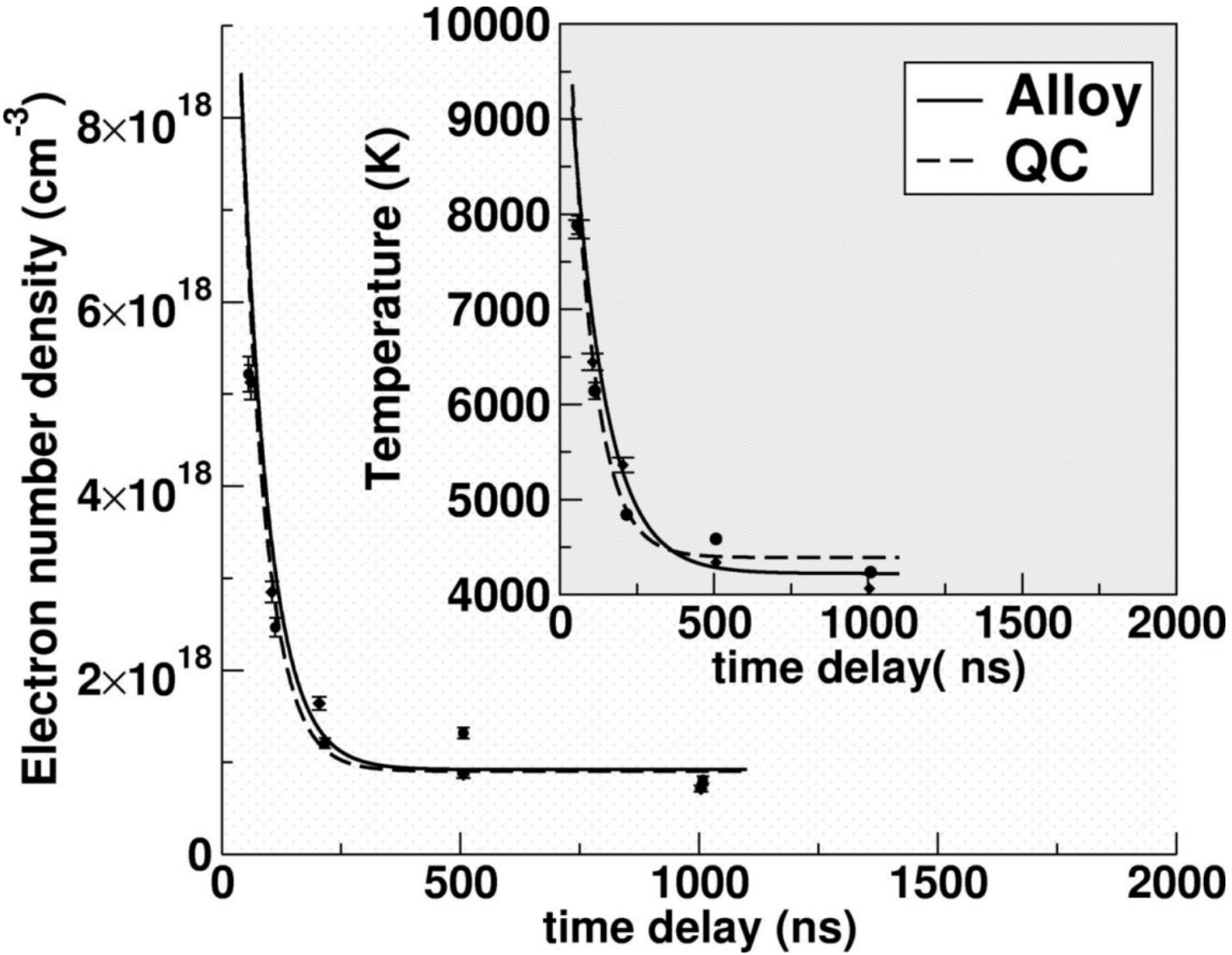
Electron number density (cm^{-3})
8×10^{18}
6×10^{18}
4×10^{18}
2×10^{18}
0
0
500
1000
1500
2000
time delay (ns)
Temperature (K)
10000
9000
8000
7000
6000
5000
4000
0
500
1000
1500
2000
time delay(ns)
Alloy
QC

Figure 7

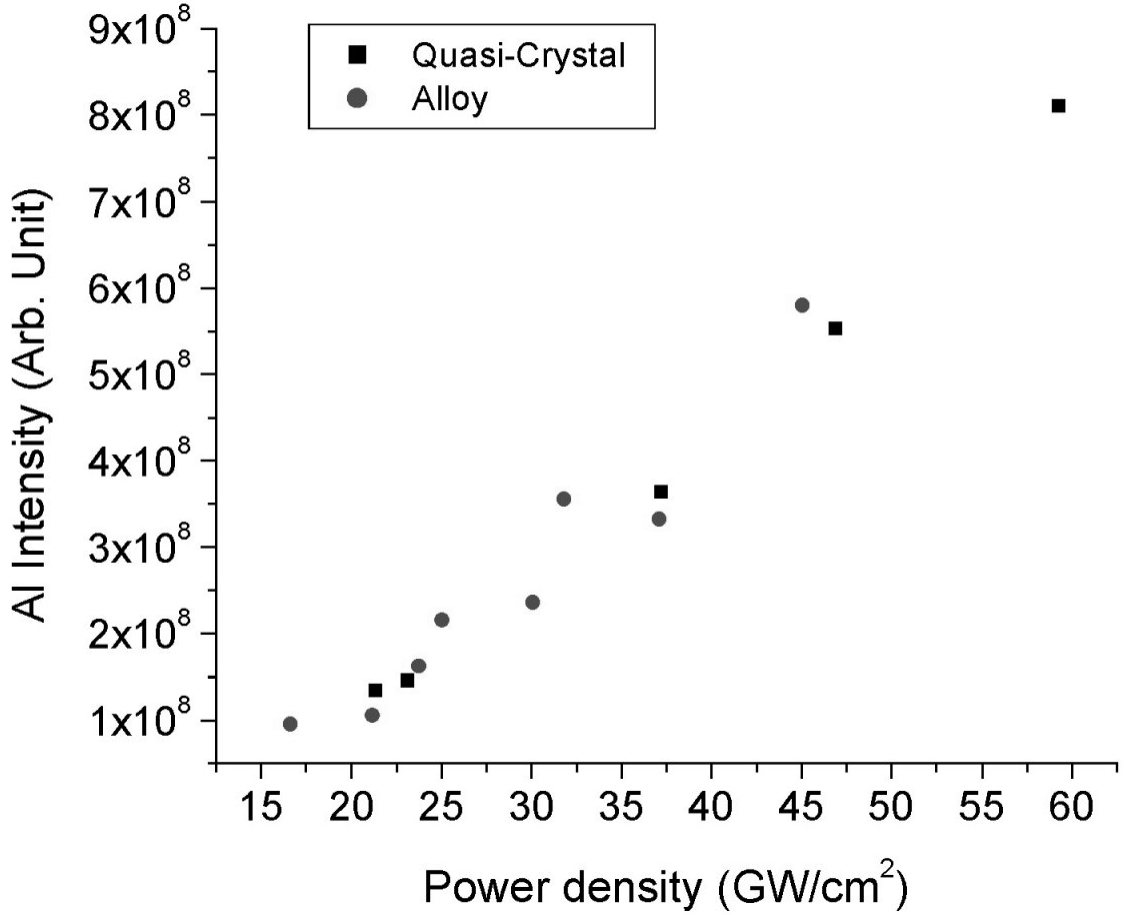
Quasi-Crystal
Alloy
Al Intensity (Arb. Unit)
9x10^8
8x10^8
7x10^8
6x10^8
5x10^8
4x10^8
3x10^8
2x10^8
1x10^8
15
20
25
30
35
40
45
50
55
60
Power density (GW/cm^2)

Figure 8